JOURNAL OF THE ROYAL SOCIETY Interface

Multi-layered bird beaks: a finite-element approach towards the role of keratin in stress dissipation

Joris Soons, Anthony Herrel, Annelies Genbrugge, Dominique Adriaens, Peter Aerts and Joris Dirckx

J. R. Soc. Interface 2012 **9**, 1787-1796 first published online 15 February 2012
doi: 10.1098/rsif.2011.0910

JOURNAL OF THE ROYAL SOCIETY Interface

J. R. Soc. Interface (2012) **9**, 1787–1796
doi:10.1098/rsif.2011.0910
Published online 15 February 2012

Multi-layered bird beaks: a finite-element approach towards the role of keratin in stress dissipation

Joris Soons[1,*], Anthony Herrel[2,3], Annelies Genbrugge[1,4], Dominique Adriaens[4], Peter Aerts[3,5] and Joris Dirckx[1]

[1]*Laboratory of Biomedical Physics, University of Antwerp, Groenenborgerlaan 171, 2020 Antwerpen, Belgium*
[2]*Département d'Ecologie et de Gestion de la Biodiversité, Museum National d'Histoire Naturelle, 57 rue Cuvier, Case postale 55, 75231 Paris Cedex 5, France*
[3]*Department of Biology, University of Antwerp, Universiteitsplein 1, 2610 Antwerpen, Belgium*
[4]*Evolutionary Morphology of Vertebrates, Ghent University, K.L. Ledeganckstraat 35, 9000 Gent, Belgium*
[5]*Department of movement and sports sciences, University of Ghent, Watersportlaan 2, 9000 Gent, Belgium*

Bird beaks are layered structures, which contain a bony core and an outer keratin layer. The elastic moduli of this bone and keratin were obtained in a previous study. However, the mechanical role and interaction of both materials in stress dissipation during seed crushing remain unknown. In this paper, a multi-layered finite-element (FE) model of the Java finch's upper beak (*Padda oryzivora*) is established. Validation measurements are conducted using *in vivo* bite forces and by comparing the displacements with those obtained by digital speckle pattern interferometry. Next, the Young modulus of bone and keratin in this FE model was optimized in order to obtain the smallest peak von Mises stress in the upper beak. To do so, we created a surrogate model, which also allows us to study the impact of changing material properties of both tissues on the peak stresses. The theoretically best values for both moduli in the Java finch are retrieved and correspond well with previous experimentally obtained values, suggesting that material properties are tuned to the mechanical demands imposed during seed crushing.

Keywords: finite-element model; beak; digital speckle pattern interferometry; bone; keratin

1. INTRODUCTION

Finite-element (FE) analysis is a popular and powerful modelling tool in engineering applications to explore the mechanical consequences of different possible designs. Recently, this technique has found its way into other applications including biomedical engineering and biology, where it is used to gain insight into the mechanical consequences of a given morphology [1–5]. One of the major advantages of FE modelling is the possibility of performing *in silico* experiments allowing the theoretical exploration of a morphospace including morphologies of extinct species [4]. Moreover, computer models allow us to compare biological shapes under exactly the same boundary conditions and size, and as such separate pure shape effects from historical or developmental constraints. In a previous study, we compared the shape of the bony core of the beak in Darwin's finches using FE analysis. The use of an FE model permitted us to remove the effects of size, which enabled us to scale the beak virtually to the same dimensions and to apply the same loading and boundary conditions [3]. Similarly, such an approach can be used to isolate the effects of the structural properties of different tissues in multi-layered structures typical of biological objects.

Bird beaks are a good example of such a multi-layered, natural composite structure. They have to meet some high-performance criteria. Indeed, some beaks need to resist large forces during biting or seed crushing, but over-engineering through addition of material may impede efficient flight capacity owing to the constraints on mass. The beak not only consists of the beak bone, but also of a surrounding dermal layer with connective tissue and a cellular layer. The latter consists of living cells that keratinize towards the outer side of the beak, leaving a hard, cornified, dead keratin layer at the outer surface of the beak [6]. Epidermis, dermis and bone are anchored to each other with collagenous Sharpey's fibres (bone–dermis interaction)

*Author for correspondence (joris.soons@ua.ac.be).

Received 27 December 2011
Accepted 27 January 2012

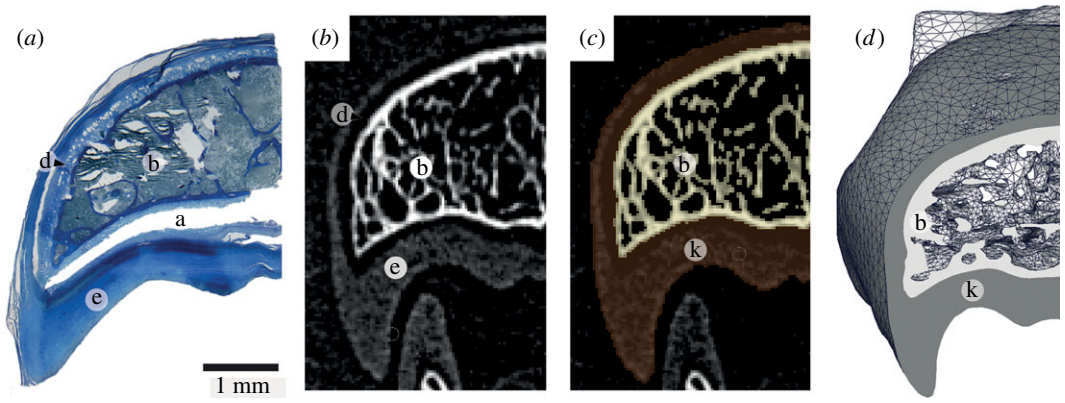

Figure 1. Transverse cross section of the Java finch upper beak. (*a*) Histological section, (*b*) CT reconstruction, (*c*) segmented CT reconstruction, and (*d*) frontal view of transversal cut FE model (see figure 2). With (a) artefact, (b) bone, (d) dermis, (e) epidermis, and (k) keratin layer in FE model.

or numerous tissue interdigitations (dermis–epidermis interaction; A.G., personal observation; in figure 1*a*). Previous work on the composite structure and the mechanical behaviour of a toucan beak was done by Seki and co-workers [7,8]. They found that the toucan beak consists of a trabecular bony core, a cortical shell and a keratin shell. An FE model successfully described the deformation and failure of a beak's section under compression. Moreover, a synergy between the foam (trabecular bone) and shell was observed: the energy absorbed by the shell and foam together is higher than the energy of both separately. In this paper, we study a granivorous bird (the Java finch), which uses its beak, in contrast to the toucan, to crush seeds. In fact our principal interest resides in the mechanical stress exerted on the beak during seed-crushing, and how the beak morphology and constituent materials are tuned to optimizing bite performance.

Therefore, we present a multi-layered FE model of the upper beak of the Java finch (*Padda oryzivora*) and validate the model using *in vivo* bite force measurements and direct measurements of the deformation of the beak *in vitro*. To do so, the full field out-of-plane displacement in the FE model is compared with that measured using digital speckle pattern interferometry (DSPI). DSPI is an accurate tool allowing the measurement of small displacements in small and complex structures such as the upper beak of the Java finch [9–13]. The FE model contains the bony core of the upper beak and an outer 'keratin' layer, which is in fact an aggregation of the epidermal and dermal layer (figure 1*b–d*). The keratin layer is attached to the beak bone and both bone and keratin FE elements share nodes at the contact zone. This multi-layered FE model allows us to explore the effects of the material properties of both tissues on the mechanical behaviour of the beak. The model geometry was based on computed tomography (CT) data, material properties were obtained previously [14] and muscle forces are obtained from dissections. An *in silico* experiment, where the elastic modulus of both bone and keratin are changed in order to minimize the maximal von Mises (VM) stress, is performed and allows us to (i) determine the theoretically ideal moduli for bone and keratin and (ii) to explore the effects of the material properties of the multi-layered upper beak on the mechanical behaviour of the bony core.

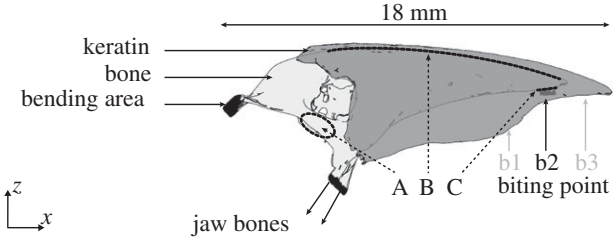

Figure 2. Sketch of the multi-component FE model of the Java finch's upper beak. In the physiological FE model, the bending area and the bite point (b2) are constrained and muscle forces are applied on the jaw bones (in the direction of the arrows). The maximum stress at four locations is recorded: posterior right and left on the nasal bone (A), on top of the upper beak's bony part (B) and at the bottom of the bony core, above the bite point (C). For the three validation FE models, both jaw bones and bending area are constrained and a force is applied at three different positions: the centre of the beak (b1), the tip of the beak (b2, natural loading position) and the rostral-most part of the keratinous upper beak (b3).

2. MATERIAL AND METHODS

2.1. Physiological finite-element model

The skull of one adult Java finch (*P. oryzivora*) specimen was scanned at the European Synchrotron Radiation Facility (ESRF, Grenoble) and 2000 × 2000 pixel images with a resolution of 45 µm were obtained. The distinction between keratin and bone was clearly visible on the reconstructed CT images (figure 1*b*) and both were segmented using semi-automatical greyscale thresholding (Amira v. 4.1; 64-bit version, TGS systems). This means that an automatic segmentation of visually selected greyscale values was followed by a manual correction to reduce artefacts. Greyscales were selected to incorporate as much material as needed (figure 1*c*). A surface model was obtained after smoothing. Although smoothing is necessary to build up an FE model, we need to take into account that it also removes small features of the model, such as the small trabeculae in the bony core (figure 1*d*). Delaunay

Table 1. Summary of muscle mass, fibre length, physiological cross-sectional area (PCSA) and force-generation capacity of the jaw adductor muscles in the Java finch ($n = 4$). Muscles indicated in black are assumed to be maximally active during the crushing of seeds (table entries are means ± s.d.).

	muscle mass (mg)	fibre length (mm)	PCSA (cm^2)	F (N)
M. depressor mandibulae	11.50 ± 2.38	3.283 ± 0.28	0.033 ± 0.01	0.820 ± 0.13
M. adductor mandibulae externus rostralis	23.38 ± 3.40	1.457 ± 0.08	0.151 ± 0.023	3.775 ± 0.59
M. adductor mandibulae externus ventralis	3.88 ± 1.03	1.275 ± 0.14	0.029 ± 0.01	0.714 ± 0.18
M. adductor mandibulae externus profundus	8.88 ± 1.93	1.345 ± 0.13	0.062 ± 0.01	1.544 ± 0.26
M. adductor mandibulae ossis quadrati	2.88 ± 1.44	1.640 ± 0.31	0.016 ± 0.01	0.408 ± 0.19
M. pseudotemporalis superficialis lateralis	3.38 ± 1.89	1.359 ± 0.48	0.023 ± 0.01	0.565 ± 0.24
M. pseudotemporalis superficialis medialis	4.38 ± 1.60	1.489 ± 0.49	0.031 ± 0.02	0.766 ± 0.41
M. pseudotemporalis profundus	7.13 ± 1.31	2.553 ± 0.49	0.027 ± 0.01	0.669 ± 0.14
M. pterygoideus ventralis lateralis	10.17 ± 2.57	2.021 ± 0.12	0.048 ± 0.01	1.190 ± 0.28
M. pterygoideus ventralis medialis	4.67 ± 2.08	2.125 ± 0.11	0.021 ± 0.01	0.518 ± 0.25
M. pterygoideus dorsalis lateralis	17.83 ± 2.75	2.018 ± 0.29	0.083 ± 0.01	2.084 ± 0.25
M. pterygoideus dorsalis medialis	7.50 ± 1.80	1.675 ± 0.26	0.042 ± 0.01	1.060 ± 0.26
M. retractor palatini	6.38 ± 1.60	2.206 ± 0.38	0.028 ± 0.01	0.697 ± 0.23
M. protractor pterygoidei et quadrati	3.75 ± 0.96	2.061 ± 0.08	0.017 ± 0.00	0.425 ± 0.10

tetrahedralization was performed in the 'TETGEN' software package [15]. After conducting the convergence test (better than 5%) for the presented results (displacement, force, VM stress), a tetrahedral grid of approximately 1188k elements was generated. This convergence test is needed to find an FE mesh that is fine enough to produce accurate results. In our case, a further refinement would have introduced a large computational cost, but would not change the results by more than 5 per cent. Next, the mesh was imported in FEBio, an FE program designed for the mechanical analysis of biological structures [16]. Subsequently, two different FE models were created: first a physiological model including natural boundary conditions and second, a validation model with the conditions of the DSPI measurements (see below).

In the physiological FE model (figure 2), the elastic modulus was set at 7.3 GPa for fresh bone and 1.7 GPa for fresh keratin. Those values were obtained in a previous study by using a double-indentation technique [14]. It was found that the modulus of keratin depends on its humidity and a modulus of 3.1 GPa was found for dry keratin. No significant difference in the modulus was detected for dry versus wet bone ($E_{\text{dry bone}} = 7$ GPa), so in this paper, a modulus of 7.3 GPa is used for both fresh and dry bone. The double-indentation technique was designed to acquire the Young modulus of thin samples. Four test materials (aluminium, PVC (polyvinyl chloride), PMMA (poly (methyl methacrylate), nylon) with different thicknesses were used to verify the proposed technique and the FE-calculated correction factor [17]. However, it should be noted that the anisotropy of bone is not considered in the model. Given the small size of these biological samples, it was impossible to measure the anisotropy experimentally. As a result, the Young modulus along the loading direction, the longitudinal axis, might be underestimated. Nevertheless, the validation measurements show a good agreement, indicating that the chosen moduli are indeed appropriate. The Poisson's ratio for both materials was set at 0.4 [18,19], although no experimentally determined values were available for avian bone and keratin. Both the beginning of the skull near the bending area and the bite point were constrained for both translation and rotation (figure 2). Constraining the bite point mimics a food reaction force. The bite point was based on *in vivo* observations of birds cracking seeds.

Muscle forces were obtained through dissection using a stereo-microscope (Olympus SZX7). For four Java finches, all jaw muscle bundles were removed individually during the dissections. Muscles were blotted dry and weighed using an OHAUS Adventurer microbalance (±0.1 mg) following Soons *et al.* [3]. Muscles were transferred to a 30 per cent aqueous nitric acid solution for 24 h to digest the connective tissue and transferred to a 50 per cent aqueous glycerol solution [20]. Fibres were teased apart using blunt-tipped glass needles and were photographed with a Nikon d40x digital camera with macro lens. Based on the digital images, the fibre lengths were measured using the software program ANALYSIS v. 5.0 (Soft Imaging System gmbH, Germany). Muscle physiological cross-sectional area (PCSA) of each muscle bundle was calculated by dividing muscle mass (g) multiplied by 1.065 g cm^{-3} (muscle density [21]) by fibre length (cm). The force-generation capacity for each muscle was calculated by multiplying the PCSA (cm^2) by 25 N cm^{-2} (muscle stress) [22]. The muscle mass, muscle fibre length, PCSA and force-generation capacity of each muscle bundles involved in jaw closing are listed in table 1. As the external adductor and pseudotemporalis muscles act only indirectly on the upper beak [23–27], the component of the muscle force transferred to the upper beak was calculated taking into account the position of the muscles and their angles relative to the jugal bone. The pterygoid muscle bundles act directly on the upper beak [23–27], and muscle forces were assumed to be directly transmitted through the pterygoid–palatine complex.

The FE model allows us to calculate the displacements of the nodes and the stresses on the elements. Stresses larger than the material strength will result in material failure. The maximum stress on the bone

of the upper beak is biologically more interesting than the stress on keratin. Indeed, as the rhamphotheca can repair itself well [28], bone fracture is much more serious. The distortion energy theory, also known as the von Mises–Hencky theory, was chosen to estimate fracture loads because it is a reliable way to overcome difficulties in the interpretation of the complex stress field [29]. The ratio of the strength of bone (σ_{u_bone}) to the peak VM stress (σ_{peak_VM}) is called the safety factor (SF). Materials with a low SF (<1) are subjected to material failure; materials with too high SFs are over-engineered and incur an extra cost in terms of material and/or energy. However, the Young modulus of a bony material can be correlated with both its strength and its density [30,31]. Fyhrie & Vashishth [31] obtained a linear relation between the Young modulus of bone (E_{bone}) and its ultimate strength (σ_{u_bone}), resulting in the following SF:

$$\mathrm{SF} = \frac{\sigma_{u\_bone}}{\sigma_{peak\_VM}} = \frac{0.0061\, E_{bone}}{\sigma_{peak\_VM}}. \tag{2.1}$$

2.2. Validation measurements

In order to validate the model output, the bite force data of five Java finches were measured using a piezoelectric force transducer (type 9203, Kistler Inc., Switzerland; ±500 N) mounted in a custom-built holder, and connected to a portable charge amplifier (Kistler, type 5059A). A detailed description of this setup is available in the study of Herrel *et al.* [32–34]. Secondly, DSPI was used to measure the displacements of the upper beak. This sensitive measurement technique precisely quantifies the out-of-plane displacement (z; figure 2) over the entire surface of this small object [9,14]. Nevertheless, our custom-made DSPI does not allow us to measure the sample three-dimensional topography and in-plane displacement components, such as the x and y (figure 2). As a consequence, we were unable to calculate the strains *in vitro*. The sensitivity of the technique also causes some practical issues. First, *in vivo* experiments are not possible. In addition, the entire setup should be placed on a vibration-isolated optical table. Applying the muscle force on the jaw bones in an experiment is very difficult. Therefore, we constrained the jaw bones and introduced a force at three different positions: the centre of the beak, the tip of the beak and the rostral-most part of the keratinous upper beak, where there is no supporting bony core (locations are indicated on figure 2). Measurements on fresh keratin gave noisy results, indicating that the nanometre stability requirement for DSPI was not totally met. This can be explained by the low light reflectance and the instability, probably owing to creep, of the surface. Therefore, the validation was performed on dry samples. The resulting reaction force was measured with a load cell (Sensotec 31, 5 N) and the resulting out-of-plane displacement, on top of the upper beak (on top of keratin) was acquired with a custom-made DSPI setup. Next, the derivative of this z-displacement (out-of-plane) along the x-direction was taken as it is a better parameter to describe bending experiments. Indeed, the derivative of a rigid body movement, which is not interesting from a mechanical point of view, will yield a constant [9,14,35]. A high-quality result is necessary to calculate this derivative, so the signal-to-noise ratio was improved by using a magnesium oxide coating to obtain a better light reflectivity and by performing each experiment 20–100 times. In order to combine these measurements, the displacements need to be divided by the imposed force. The upper beaks of three individuals were loaded on three different locations (b1, b2 and b3 in figure 2). Finally, the results for these three Java finches were averaged. As those beaks have approximately the same size, an average value could be calculated. The experimental setup was described in detail in a previous paper where it was used to obtain the moduli of upper beak bone and keratin through an inverse analysis [14].

2.3. Validation finite-element model

The geometry of the FE model was established as described above (see physiological FE model and figure 2). The constraints, the applied forces and the material properties, however, are different for this validation FE model. The beginning of the skull, near the bending zone, and the jaw bones were both constrained for translation and rotation (the constrained elements are black in figure 2). A loading (the virtual reaction force) was introduced by applying a 1 N force on the corresponding elements at the bite position. In this way, we work around the experimental difficulties of applying the muscle forces on the jaw bones. The elastic modulus of dry bone and dry keratin was obtained previously [14]: $E_{bone} = 7.3$ GPa and $E_{keratin} = 3.1$ GPa. In order to check the quality of the FE results, a coefficient of determination between the derivative of the displacement from the FE models and from the DSPI measurements was calculated. The following formula was used, with $\mathrm{Exp}(q_i)$ being the experimentally obtained values and $\mathrm{FE}(q_i)$ being the corresponding model output:

$$R^2 = 1 - \frac{\mathrm{SS_{err}}}{\mathrm{SS_{tot}}}, \tag{2.2}$$

$$\mathrm{SS_{err}} = \sum_{i=1}^{N} (\mathrm{Exp}(q_i) - \mathrm{FE}(q_i))^2, \tag{2.3}$$

$$\mathrm{SS_{tot}} = \sum_{i=1}^{N} (\mathrm{Exp}(q_i) - \mathrm{Exp})^2 \tag{2.4}$$

and

$$\mathrm{Exp} = \frac{1}{N} \sum_{i=0}^{N} \mathrm{Exp}(q_i). \tag{2.5}$$

For nonlinear regression, this coefficient of determination does not equal the square of the correlation coefficient. If the experimental values coincide with the model values ($\mathrm{Exp}(q_i) = \mathrm{FE}(q_i)$), R^2 will be 1. R^2 smaller than 0 indicates that the model prediction is less accurate as the mean of the observed data.

In this full-field calculation, the bending area and the resulting constant offset were ignored. Owing to constraint errors near the bending area, an additional rigid body movement was introduced over the entire sample. This rigid body movement added an additional linear offset to the z-displacement, which became a constant offset after derivation. This constant

Table 2. Bite force at the tip of the beak measured *in vivo* (*Padda* 1–5), the average for the five specimens (±s.d.) and the corresponding bite force derived from the physiological FE model are also given.

	Padda 1	*Padda* 2	*Padda* 3	*Padda* 4	*Padda* 5	average	FE model
tip bite force (N)	9.7	7.5	9.3	8.7	10	9.0 ± 0.9	6.8

offset was ignored so that rigid body movements, which are uninteresting from a mechanical point of view, were neglected.

2.4. Surrogate model: which moduli for bone and keratin are 'the best'?

We wanted to explore how the elastic moduli for bone and keratin affect the peak stress in the entire upper beak. Moreover, we wanted to find which pair of moduli gives the lowest stress, and can thus be considered as 'the best'. Insights can be gained using a surrogate model. Such a surrogate model will yield a peak stress of the upper beak FE model for a given modulus of bone and keratin. Therefore, the FE model is calculated for several pairs of moduli and one obtains a surrogate model as presented in §3 (figure 4).

In our FE model, both the bony core and the keratin layer were modelled as linear elastic materials. The Young modulus of both materials is the input variable for our model. The moduli can be changed and a corresponding output is obtained. As output, the peak VM stress in four different regions of the upper beak FE model was recorded: at the bottom of the bone close to the bite point (A, figure 2), on top of the bone (B), and posterior right and left on the nasal bone (C). Areas with high stresses close to areas that are constrained in the model, such as the bending area, were ignored. Four surrogate models were established to connect a set of elastic moduli of bone and keratin with the peak VM stresses for the four selected locations recorded at the level of the bone. Afterwards, an optimal set of moduli, which yield a minimal peak VM stress, was selected and the impact of the elastic moduli on stress was examined.

3. RESULTS

3.1. Validation measurements

The first validation of our FE model consists of comparing the *in vivo* bite force with the one obtained in the physiological FE model. The results for tip loading of five Java finches and its average are presented in table 2. An average of 9 ± 1 N for five Java finches was measured. In the FE model, we obtained the vectorial components of the forces *Fx*, *Fy*, *Fz* = 2.2, 0, 6.5 N, resulting in a total bite force of 6.8 N, which is somewhat lower, yet reasonably close to the observed *in vivo* bite forces.

In figure 3, we show the cross-sectional results[1] for the bending experiments performed on three different

[1]Results on top of the upper beak, lying on a line from the tip of the beak to its articulation with the skull (y being constant, x ranging from 0 to 20 mm).

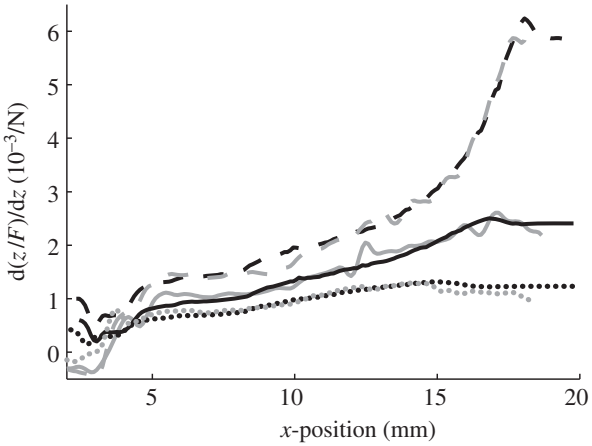

Figure 3. Results of the validation measurements. Black lines indicate the results of the validation FE model, grey lines the average (of three specimens) of the corresponding bending experiments. Dashed lines represent a loading at the rostral-most part of the keratinous upper beak ($R^2 = 0.97$), full lines represent tip loading ($R^2 = 0.89$) and dotted lines represent centre loading ($R^2 = 0.89$).

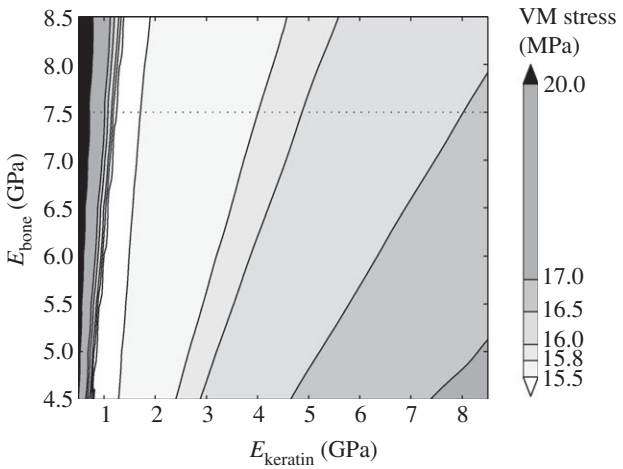

Figure 4. Peak VM stress (MPa) in bone for different moduli of the bony core (E_{bone}) and the keratin layer ($E_{keratin}$).

locations of the beak. Black lines indicate the derivative of the z-displacement along the x-direction of the validation FE models. Grey lines represent the average value of the corresponding DSPI measurements on three different Java finches. Full lines represent the results for tip loading (b2 in figure 2), the dotted lines represent a loading at the centre of the beak (b1 in figure 2) and the dashed lines are the results from a loading at the rostral-most part of the keratinous upper beak (b3 in figure 2). For tip-loading, an R^2 of 0.97 is found and for centre and total tip-loading, an R^2 of 0.89 is obtained suggesting that the FE

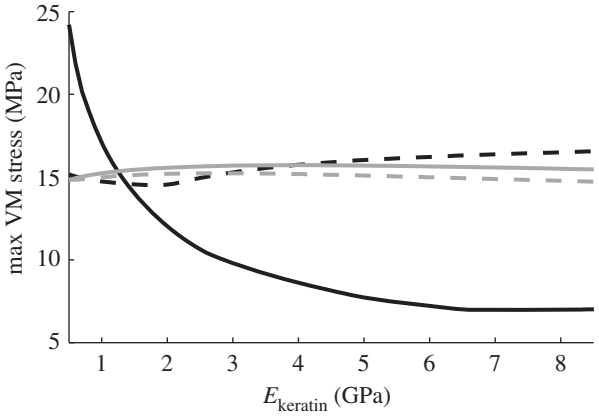

Figure 5. Peak VM stress results following the dotted line in figure 4 (as a function of the keratin modulus, for a fixed $E_{bone} = 7.5$ GPa) at four different positions on the bone: on top (solid black line), at bite position (dashed black line), posterior right (solid grey lines) and left (dashed grey lines) (as indicated in figure 2).

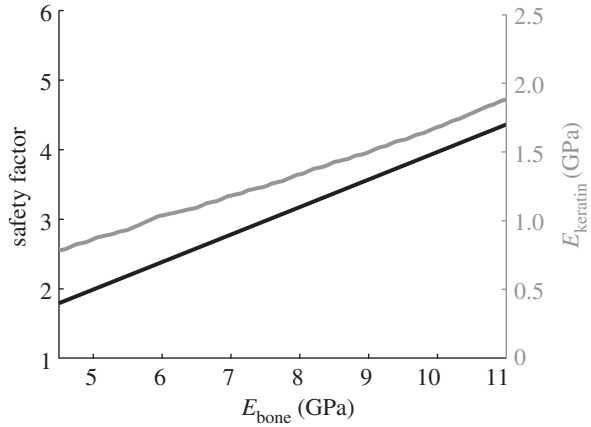

Figure 6. The relationship between the modulus of bone (E_{bone}) and the corresponding modulus of keratin ($E_{keratin}$) used to find the minimal peak VM stress in the model (grey line) and the SF of this corresponding minimum (black line) (see equation (2.1)).

model provides a good representation of the *in vitro* displacement of the actual biological material.

3.2. Surrogate model

The surrogate model, relating the Young modulus of bone and keratin with the maximal VM stress in bone is presented in figure 4. The maximal stress is obtained by calculating the maximum of the stress at the four selected locations (A, B and C in figure 2). The curves in figure 5 are the peak VM stress (y-axis) on those four selected locations for a constant bone modulus of 7.5 GPa and a changing keratin modulus (x-axis) and represent the results along the dotted line in figure 4. The peak VM stress, however, hardly changes for different moduli of bone. Nevertheless, it is known from equation (2.1) that the strength and modulus of bone are linearly correlated, resulting in a strength of 45 MPa for a Young modulus of 7.3 GPa. Consequently, a linear fit between the SF for bone and its modulus is also found (equation (2.1)). Therefore, the SF of bone is plotted as function of its modulus in figure 6.

The smallest peak VM stresses of approximately 15 MPa are found in an oblique valley in the surrogate model, with keratin moduli ranging from 0.8 to 1.9 GPa (figure 4). When looking at different bone moduli, one will find slightly different keratin moduli to obtain the minimal peak VM stress ($\pm$15 MPa). For example, the minimal peak VM stress for a bone modulus of 5 GPa is found for a keratin modulus of 0.9 GPa. For a bone modulus of 11 GPa, an 1.8 GPa keratin modulus is found. This pair of optimal values for the modulus of bone and keratin is also shown as the grey line in figure 6.

As an example, three FE models of the Java finch with natural loading conditions are presented in figure 7. The Young modulus of bone in all these models is 7.5 GPa. Three different moduli for keratin are chosen: $E_{keratin} = 0.5$, 1.6 and 6.5 GPa. The colour plot indicates the resulting VM stress on bone with warmer colours representing higher VM stresses. Finally, we also indicate the resulting force at the bite point. For softer keratin, this force is directed more towards the back of the beak. For $E_{keratin} = 0.5$, 1.6 and 6.5 GPa, we found forces of 7.5, 6.8 and 6.6 N, respectively, with lower Young's moduli being associated with higher forces.

4. DISCUSSION

4.1. Validation measurements

The beak is a complex, composite structure (figure 1) and some approximations are necessary to create a mechanical model of it. First the epidermal and dermal layers are modelled as one homogeneous, isotropic and linear elastic keratin layer. Second, both the cortical and the cancellous bone are modelled as homogeneous and isotropic. An elastic modulus of the cortical bone layer was obtained in a previous paper [14]. The cancellous bone does not appear to be homogeneous at all. It forms struts at some regions and in other regions almost no bone is found. Moreover, such struts are too small for mechanical testing. Another inaccuracy is the overestimation of cortical and trabecular bone thickness (compare figure 1*d* with figure 1*a*,*b*) owing to the semi-automatic segmentation. Additionally, after smoothing, only the largest struts are left in our model. Finally, the connection between the keratin and bone is modelled as if they are fully attached with each other.

Those approximations can have an impact on the mechanical behaviour of the model and therefore, a validation procedure is an important component of a good FE model. Two experiments are conducted. In the first one, we compared the resulting bite force calculated in the model with bite force measured *in vivo*. A lower bite force is obtained in the FE model, but the relative difference with the average value of five *in vivo* samples is smaller than 25 per cent (note that the difference with *Padda* 2, for example, is less than 10%). This result seems to be acceptable as the mean relative

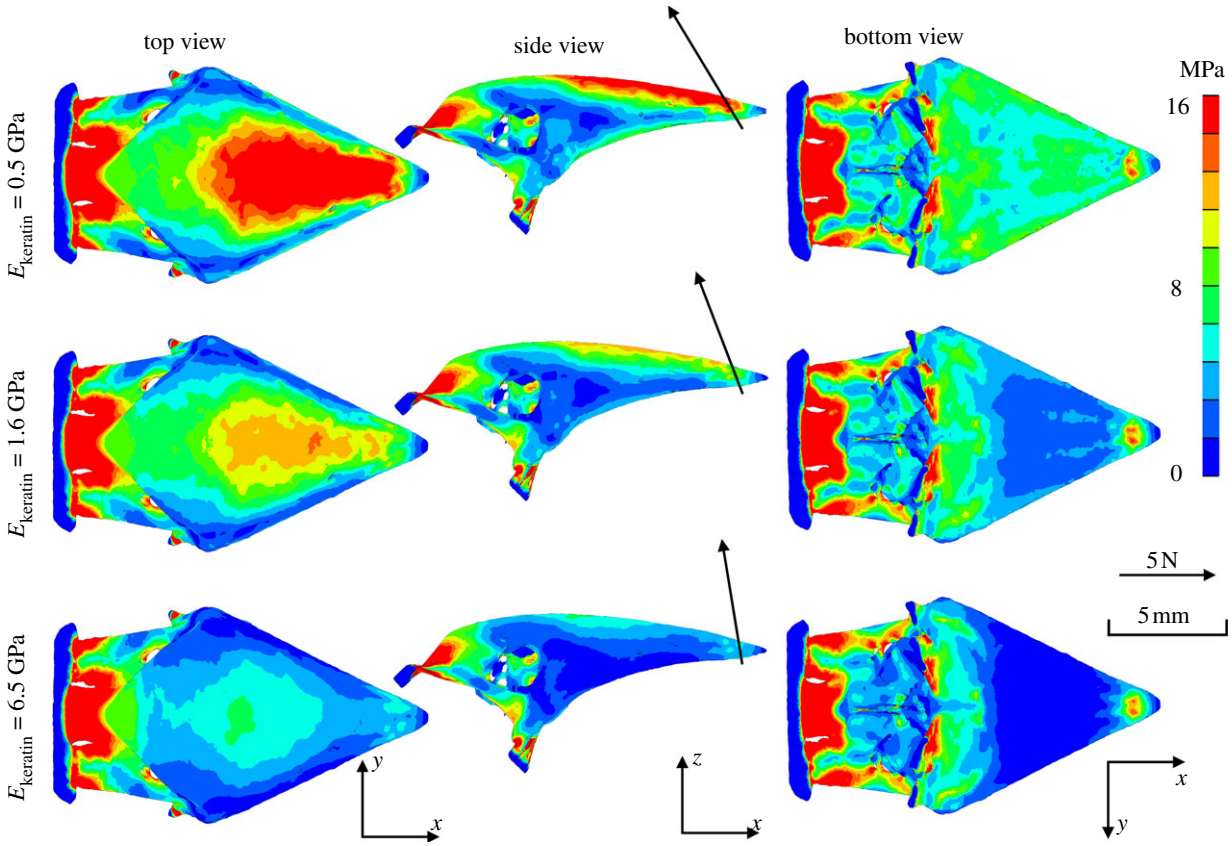

Figure 7. Top, side and bottom view of the VM stress on the bony core of the upper beak of the Java finch, for $E_{bone} = 7.5$ GPa and $E_{keratin} = 0.5$ GPa (first row), 1.6 GPa (second row) and 6.5 GPa (third row). Note that the keratin layer is not shown. The resulting bite force is also presented.

standard deviation of the model input forces (table 1) is almost 30 per cent because of variation in muscle cross-sectional area in the individuals examined. In addition, preliminary results on Darwin's finches show that there is no systematic over- or underestimation of bite force. Hence, the model and the chosen boundary conditions appear realistic. However, several FE models, with different stress fields, will produce similar forces (figure 7) and thus ideally additional validation measurements are required.

In this paper, the derivative of the z-displacement (out-of-plane) along the x-direction, obtained with DSPI is compared with the outcome of our FE model. This interferometric technique offers some major advantages over conventional methods such as strain gauges. It is a non-contact method allowing us to quantify deformation of the small and complex upper beak. Furthermore, the method is full-field, yielding a better validation. The major drawback of DSPI is its sensitivity, which makes *in vivo* experiments unfeasible and makes measurements on fresh samples difficult [9,14]. This practical issue is overcome by introducing a bending experiment on a dry sample on three different locations. The signal-to-noise ratio of the experimental results is improved by using the average of multiple measurements. In addition, the measurements on three Java finches are combined. The coefficient of determination (R^2) for the three different locations is greater than 0.89, indicating a good fit of the model to the data points and thus validating our FE model. This goodness of fit for the three different loading conditions can also be observed in figure 3. It should be noticed that there is a discrepancy at the bending area, which is the zone with x-values smaller than 5 mm in figure 3. This may be owing to an approximation in the modelling. We believe that this bending area consists of less dense and less stiff bone. Therefore, the displacement at this position and the additional rigid body movement of the entire sample is ignored. In addition, the VM stress is not being recorded in this region, because a much larger stress is expected because of the absence of the supporting bone of the skull in the model.

In conclusion, both validation measurements indicate that our FE model provides reliable and biologically pertinent data. Consequently, we can alter variables in the model, and perform an *in silico* experiment. More specifically, we are interested in the relation between the elastic moduli of keratin and bone and the resulting SF of the bone. These data also provide insights into the biological role of the keratin layer that is present on the beak of birds.

4.2. Surrogate model: which moduli for bone and keratin are 'the best'?

The surrogate model in figure 4 shows the highest peak VM stress on the four selected regions for every modulus of bone and keratin (figure 2). This peak VM stress is an important value to obtain the SF

(equation (2.1)). We will first explore the influence of the keratin modulus on this peak VM stress. Therefore, the bone modulus is fixed at 7.5 GPa and the keratin modulus is changed. The peak VM stress is recorded at four different regions (indicated as A, B and C on figure 2) and are shown in figure 5. As an example, the FE models for this bone modulus of 7.5 GPa and for keratin moduli of 0.5, 1.6 and 6.5 GPa are presented in figure 7.

On the bottom view of figure 7, differences between the different models for the maximum VM stress close to the bite point (C in figure 2) are barely visible. This behaviour can also be seen in figure 5, represented by an almost horizontal, black dashed line.

The peak VM stresses posterior right and left on the nasal bone (A in figure 2) also seem to be largely independent of variation in the keratin modulus (both grey lines in figure 5).

On the top view of figure 7, however, one can see a large variation in stress for the three models. A smaller elastic modulus for keratin will result in a higher peak stress on top of the upper beak and vice versa. This relationship is also visible upon inspection of the black line in figure 5. In addition, the FE models show a shift of the position of the peak stress region. Indeed, increasing the keratin modulus (e.g. from 1.6 to 6.5 GPa) will shift the peak stress on top of the upper beak from the tip more to the centre of the beak. In general, for all recorded locations, one can see a rapid increase in peak VM stress for keratin moduli smaller than 1 GPa (black line in figure 5) and an almost flat relation for moduli larger than 1.7 GPa (dotted and grey lines in figure 5). On the other hand, increasing the modulus of keratin probably has an effect on its density [30], which introduces a limiting factor for high keratin moduli. For a bone modulus of 7.5 GPa, a keratin modulus of approximately 1.3 GPa appears to be optimal if we assume a requirement of a minimal peak VM. It is clear that the value of the keratin modulus has an impact on the VM stress detected at the level of the bony core, indicating the importance of selecting proper material properties in a multi-component FE model. The results also emphasize the biological role of keratin in complex multi-layered structures such as bird beaks. Indeed, the resulting bite force of the three FE case studies differs slightly in magnitude and orientation. A stiffer keratin modulus results in a smaller bite force. More interestingly, the direction of the bite force is more perpendicular to the biting surface for stiffer keratin. As a consequence, shear forces are kept minimal.

Finally, we examined the dependency of the VM stress upon the bone modulus. In the surrogate model (figure 4), a minimal VM stress of approximately 15 MPa is found for every bone modulus. This minimal VM stress has a slightly different keratin modulus for every bone modulus (see grey line in figure 6). Nevertheless, one can expect a change in the bone strength for the different bone moduli and thus a change in the SF. Indeed, the material strength is, besides the peak VM stress, also an important value to obtain the SF. Literature values for cortical bone strengths range from 106 to 244 MPa over a wide range of vertebrates [36–38]. On the other hand, a close correlation between Young's modulus, density and strength of both cortical as well as cancellous bone has been proposed [31], resulting in a strength that linearly depends on the modulus (e.g. 45 MPa for a Young modulus of 7.3 GPa). Consequently, the SF corresponding to a certain modulus of bone can be obtained using equation (2.1). The results for the surrogate model are plotted as the black line in figure 6. Blob & Biewener [39] summarized SFs for biological materials that ranged between 2 and 4 for tetrapod limb bones. Therefore, we supposed an SF of 3 for the upper beak bone [39], resulting in a bone modulus of 7.5 GPa and a corresponding keratin modulus of 1.3 GPa. The moduli correspond well with those obtained experimentally in a previous paper, namely $E_{\text{bone}} = 7.3 \pm 0.6$ and $E_{\text{ker}} = 1.7 \pm 0.4$ GPa [10].

The absolute results reported here should be treated with some care. First, the linear relation between bone strength and modulus, obtained by Fyhrie & Vashishth [31], has never been tested for avian bone. The linear relationship is acquired for standardized test on both cortical bone and cancellous bone samples. In our case, the cancellous and cortical bone are not separately loaded, but in parallel. As a consequence, this linear relation may not be met, but a similar correlation between modulus, strength and density can be expected. Moreover, we presumed an SF of 3, but the exact value remains unknown. Nevertheless, even despite those assumptions, the relative outcome and our conclusion remains valid.

In conclusion, it was shown that the constituent materials of multi-layered bird beaks are well-tuned for biting. Indeed, the physiological elastic modulus of bone and keratin yields the lowest peak stress during bending. On the other hand, our model shows that higher moduli, probably increasing the beaks' mass, have no effect on the maximal stress. As a result, the whole construction results in a high stiffness to weight ratio. In normal sandwich-structured composition for instance, this high stiffness to weight ratio is achieved by a high elastic modulus of the face-sheets. In the Java finch's beak, a foam-structured spongy bone in the centre is also surrounded by stiffer compact bone. But, an extra, softer keratin layer surrounds the brittle bony core, potentially to protect it from impact loading for instance. This brittle behaviour was observed by removing the keratin layer in the validation experiment. A similar loading as used before, resulted in the rupture of the bony core. For impact loadings, the time-dependent properties of the material parameters will become important and thus the mechanical behaviour may be significantly different when compared with static loading cases. Dynamic and transient loading experiments are needed to investigate the behaviour of the system when it is subjected to impact forces, and this will be the subject for further research. Nevertheless, our results indicate that morphology and material parameters are well suited to support bending and therefore to perform tip biting in the Java finch.

Financial support to this project is given by the Research Foundation–Flanders (FWO) to J.S. and by an

interdisciplinary research grant of the special research fund of the University of Antwerp to J.S., J.D., P.A., A.G. and A.H. and a PHC Tournesol grant to A.H. and D.A. We thank F. Wiese and W. Deblauwe for their technical assistance.

REFERENCES

1 Dumont, E. R., Piccirillo, J. & Grosse, I. R. 2005 Finite-element analysis of biting behavior and bone stress in the facial skeletons of bats. *Anat. Rec. A* **283**, 319–330. (doi:10.1002/ar.a.20165)

2 Reed, D. A., Porro, L. B., Iriarte-Diaz, J., Lemberg, J. B., Holliday, C. M., Anapol, F. & Ross, C. F. 2011 The impact of bone and suture material properties on mandibular function in *Alligator mississippiensis*: testing theoretical phenotypes with finite element analysis. *J. Anat.* **218**, 59–74. (doi:10.1111/j.1469-7580.2010.01319.x)

3 Soons, J., Herrel, A., Genbrugge, A., Aerts, P., Podos, J., Adriaens, D., de Witte, Y., Jacobs, P. & Dirckx, J. 2010 Mechanical stress, fracture risk and beak evolution in Darwin's ground finches (*Geospiza*). *Phil. Trans. R. Soc. B* **365**, 1093–1098. (doi:10.1098/rstb.2009.0280)

4 Rayfield, E. J. 2007 Finite element analysis and understanding the biomechanics and evolution of living and fossil organisms. *Annu. Rev. Earth Planet Sci.* **35**, 541–576. (doi:10.1146/annurev.earth.35.031306.140104)

5 Ross, C. F., Berthaume, M. A., Dechow, P. C., Iriarte-Diaz, J., Porro, L. B., Richmond, B. G., Spencer, M. & Strait, D. 2011 *In vivo* bone strain and finite-element modeling of the craniofacial haft in catarrhine primates. *J. Anat.* **218**, 112–141. (doi:10.1111/j.1469-7580.2010.01322.x)

6 Van Hemert, C., Handel, C. M., Blake, J. E., Swor, R. M. & O'Hara, T. 2011 Microanatomy of passerine hard-cornified tissues: beak an claw structure of the Black-capped chickadee (*Poecile atricapillus*). *J. Morphol.* **273**, 226–240. (doi:10.1002/jmor.11023)

7 Seki, Y., Schneider, M. & Meyers, M. 2005 Structure and mechanical behavior of a toucan beak. *Acta Mater.* **53**, 5281–5296. (doi:10.1016/j.actamat.2005.04.048)

8 Seki, Y., Mason, M. & Meyers, M. A. In press. Structure and micro-computed tomography-based finite element modeling of toucan beak. *J. Mech. Behav. Biomed.* (doi:10.1016/j.jmbbm.2011.08.003)

9 Soons, J. & Dirckx, J. J. J. 2010 Full field displacement and strain measurement of small complex bony structures with digital speckle pattern interferometry and shearography. *Proc. SPIE, Florianopolis* **7387**, 73870C.

10 Gröning, F., Liu, J., Fagan, M. J. & O'Higgins, P. 2009 Validating a voxel-based finite element model of a human mandible using digital speckle pattern interferometry. *J. Biomech.* **42**, 1224–1229. (doi:10.1016/j.jbiomech.2009.03.025)

11 Panagiotopoulou, O., Curtis, N., O' Higgins, P. & Cobb, S. N. 2010 Modelling subcortical bone in finite element analyses: a validation and sensitivity study in the macaque mandible. *J. Biomech.* **43**, 1603–1611. (doi:10.1016/j.jbiomech.2009.12.027)

12 Bright, J. A. & Gröning, F. 2011 Strain accommodation in the zygomatic arch of the pig: a validation study using digital speckle pattern interferometry and finite element analysis. *J. Morphol.* **272**, 1388–1398. (doi:10.1002/jmor.10991)

13 Panagiotopoulou, O., Kupczik, K. & Cobb, S. N. 2011 The mechanical function of the periodontal ligament in the macaque mandible: a validation and sensitivity study using finite element analysis. *J. Anat.* **218**, 75–86. (doi:10.1111/j.1469-7580.2010.01257.x)

14 Soons, J., Herrel, A., Aerts, P. & Dirckx, J. 2012 Determination and validation of the elastic moduli of small and complex biological samples. *J. R. Soc. Interface* **9**, 1381–1388. (doi:10.1098/rsif.2011.0667)

15 Si, H. 2006 *TetGen: a quality tetrahedral mesh generator and three-dimensional Delaunay triangulator, User's manual, v. 1.4*. See http://tetgen.berlios.de/.

16 Maas, S. & Weiss, J. A. 2008 FEBio: finite elements for biomechanics, User's manual, v. 1.0. See http://mrl.sci.utah.edu/software/febio.

17 Soons, J. A. M., de Baere, I. & Dirckx, J. J. J. 2011 New double indentation technique for measurement of the elasticity modulus of thin objects. *Exp. Mech.* **51**, 85–95. (doi:10.1007/s11340-010-9340-8)

18 Franck, A., Cocquyt, G., Simoens, P. & Belie, N. D. 2006 Biomechanical properties of bovine claw horn. *Biosys. Eng.* **93**, 459–467. (doi:10.1016/j.biosystemseng.2006.01.007)

19 Wroe, S. 2008 Cranial mechanics compared in extinct marsupial and extant African lions using a finite-element approach. *J. Zool.* **274**, 332–339. (doi:10.1111/j.1469-7998.2007.00389.x)

20 Loeb, G. E. & Gans, C. 1986 *Electromyography for experimentalists*. Chicago, IL: University of Chicago Press.

21 Méndez, J. & Keys, A. 1960 Density and composition of mammalian muscle. *Metabolism* **9**, 184–188.

22 Nigg, B. & Herzog, W. 2007 *Biomechanics of the musculo-skeletal system*, 3rd ed. UK: University of Calgary, John Wiley & Sons Ltd.

23 Bowman, R. I. 1961 *Morphological differentiation and adaptation in the Galapagos finches*. Berkeley and Los Angeles: University of California Press.

24 Nuijens, F. & Zweers, G. 1997 Characters discriminating two seed husking mechanisms in finches (Fringillidae: Carduelinae) and Estrildids (Passeridae: Estrildinae). *J. Morphol.* **232**, 1–33. (doi:10.1002/(SICI)1097-4687(199704)232:1<1::AID-JMOR1>3.0.CO;2-G)

25 van der Meij, M. & Bout, R. 2004 Scaling of jaw muscle size and maximal bite force in finches. *J. Exp. Biol.* **207**, 2745–2753. (doi:10.1242/jeb.01091)

26 van der Meij, M. & Bout, R. 2008 The relationship between shape of the skull and bite force in finches. *J. Exp. Biol.* **211**, 1668–1680. (doi:10.1242/jeb.015289)

27 Genbrugge, A., Herrel, A., Boone, M., Van Hooreneke, L., Podos, J., Dirckx, J., Aerts, P. & Adriaens, D. 2011 The head of the finch: the anatomy of the feeding system in two species of finches (*Geospiza fortis* and *Padda oryzivora*). *J. Anat.* **219**, 676–695. (doi:10.1111/j.1469-7580.2011.01437.x)

28 Homberger, D. G. & Brush, A. H. 1986 Functional-morphological and biochemical correlations of the keratinized structures in the African gray parrot, *Psittacus erithacus* (AVES). *Zoomorphology* **106**, 103–114. (doi:10.1007/BF00312112)

29 Keyak, J. H. & Rossi, S. A. 2000 Prediction of femoral fracture load using finite element models: an examination of stress- and strain-based failure theories. *J. Biomech.* **33**, 209–214. (doi:10.1016/S0021-9290(99)00152-9)

30 Bonser, R. H. C. 2001 The mechanical performance of medullary foam from feathers. *J. Mater. Sci. Lett.* **20**, 941–942. (doi:10.1023/A:1010993219791)

31 Fyhrie, D. P. & Vashishth, D. 2000 Bone stiffness predicts strength similarly for human vertebral cancellous bone in compression and for cortical bone in tension. *Bone* **26**, 169–173. (doi:10.1016/S8756-3282(99)00246-X)

32 Herrel, A., Podos, J., Huber, S. K. & Hendry, A. P. 2005 Evolution of bite force in Darwin's finches: a key role for

head width. *J. Evol. Biol.* **18**, 669–75. (doi:10.1111/j.1420-9101.2004.00857.x)

33 Herrel, A., Podos, J., Huber, S. K. & Hendry, A. P. 2005 Bite performance and morphology in a population of Darwin's finches: implications for the evolution of beak shape. *Funct. Ecol.* **19**, 43–48. (doi:10.1111/j.0269-8463.2005.00923.x)

34 Herrel, A., Spithoven, L., van Damme, R. & de Vree, F. 1999 Sexual dimorphism of head size in *Gallotia galloti*: testing the niche divergence hypothesis by functional analyses. *Funct. Ecol.* **1**, 289–297. (doi:10.1046/j.1365-2435.1999.00305.x)

35 Leendertz, J. & Butters, J. N. 1973 An image-shearing speckle-pattern interferometer for measuring bending moments. *J. Phys. E* **6**, 1107–1110. (doi:10.1088/0022-3735/6/11/019)

36 Yamada, H. 1970 *Strength of biological materials*. Baltimore, MD: Williams & Wilkins.

37 Vogel, S. 2003 *Comparative biomechanics: life's physical world*. Princeton, NJ: Princeton University Press.

38 Currey, J. D. 2006 *Bones: structure and mechanics*. Princeton, NJ: Princeton University Press.

39 Blob, R. & Biewener, A. 1999 *In vivo* locomotor strain in the hindlimb bones of *Alligator mississippiensis* and *Iguana iguana*: implications for the evolution of limb bone safety factor and non-sprawling limb posture. *J. Exp. Biol.* **202**, 1023–1046.